insure this; hence, if $B_0 = 5.0$ the wake strength parameter Π must equal 0.35 (see Fig. 2), which shows Δu_+. Note the excellence of Nikuradse's data. At values of $k_+ > 40$, the curve tends well to the line of slope 5.616. Evidently, if data for smooth pipes with the same bore and discharge rates as those of the rough pipes had been available, κ could have been found from measurements of the discharge rate and pressure gradient alone.

Discussion

Hinze (Ref. 2, p. 718) suggests that the constant A in $u_+ = A\ell nz_+ + B$ varies with R_n in the case of pipes: "Not withstanding the great scatter of the data a trend of the values of A and B as a function of R_n appeared noticeable. The general trend of the parameter A is to increase with increasing R_n for both smooth and rough pipes, with a tendency to level off at $R_n = 10^6$."

Tennekes and Lumley (Ref. 6, p. 176) also suggest that A in a pipe increases at large Reynolds numbers toward a limiting value of three. Their experimental data reach values of ru_τ/ν of 5×10^5, corresponding with Colebrook's measurements on the penstocks of the Niagara Falls power station. Yet a reanalysis of Colebrook's measurements[7] up to $R_n = 3 \times 10^7$ shows that they are consistent with a Coles-type velocity profile with $\kappa = 0.41$.

Hinze's conclusion was based on Nikuradse's pipe work. It is suggested that the trend in A was due to nothing more unusual than that the influence of the wake term and of the inevitable errors in the origin has not been taken into account.

Conclusions

1) Nikuradse's results for pipes coated with sand are consistent with Coles' velocity profile and with the value 0.41 of the Karman constant.

2) Nikuradse's measurements on rough pipes give no evidence for a Karman constant that varies with Reynolds number.

3) Accurate values of the Karman constant cannot be determined from the slope of the logarithmic part of the velocity profile since there is no independent way to find the errors of origin.

Acknowledgments

Dr. A.K. Lewkowicz of Liverpool University and Dr. A.J. Musker of the Admiralty Marine Technology Establishment, Haslar, England, are warmly thanked for valuable discussions.

References

[1] Nikuradse, J., "Laws of Flow in Rough Pipes," NACA TM 1292.

[2] Hinze, J.O., *Turbulence,* 2nd Ed., McGraw Hill Book Co., New York, 1975.

[3] Coles, D., *The Young Person's Guide to the Data,* Vol. II, AFOSR-IFP Stanford Conference on the Calculation of Turbulent Boundary Layers, 1968.

[4] Einstein, H.A. and El-Samni, El-S.A., "Hydrodynamic Forces on a Rough Wall," *Reviews of Modern Physics,* Vol. 21, 1949, pp. 550-524.

[5] Coles, D., "The Law of the Wake in the Turbulent Boundary Layer," *Journal of Fluid Mechanics,* Vol. 1, 1956, pp. 191-226.

[6] Tennekes, H. and Lumley, J.L., *A First Course in Turbulence,* MIT Press, Cambridge, Mass., 1972.

[7] Grigson, C.W.B., "The Drag Coefficients of a Range of Ship Surfaces, II," published for written discussion by the Royal Institute of Naval Architects, London, Paper W4, 1982.

Prediction of Transonic Separated Flows

C. C. Horstman* and D. A. Johnson†
NASA Ames Research Center
Moffett Field, California

Introduction

ALTHOUGH considerable advances have been made in the prediction of the flow over supercritical airfoils, the accuracy deteriorates as the shock wave becomes stronger and eventually separates the boundary layer with increasing angle of attack or Mach number. A recent investigation by the authors[1] provided a detailed comparison between a thoroughly documented transonic flow with shock-induced separations and solutions of the flow using the Navier-Stokes equations. Although the overall flowfield was reasonably predicted, there were several deficiencies in the computations; namely, the failure to predict shock location and the proper extent and size of the separation. New experimental data in a larger wind tunnel have been obtained with the same test model for a wider range of freestream Mach numbers. The recent results indicate that the former data were free from wind tunnel wall effects and have caused the authors to re-examine the previous numerical solutions which employed solid wall boundary conditions. Futhermore, the new data provide a more realistic test for the computation method since they provide trends with varying Mach number.

The purpose of this Note is to inform the reader of the new data, to show results of new Navier-Stokes computations using more compatible boundary conditions, and to assess the effects of the turbulence model choice on predicting Mach number trends.

Experiment

The test model described in Ref. 1 consisted of thin-walled cylinder, 15.2 cm o.d., with an axisymmetric circular arc bump attached 61 cm from the cylinder leading edge. The bump had a thichness of 1.9 cm and a chord length c of 20.3 cm. The streamwise distance x referred to in this Note is the distance from the leading edge of the bump. The present data were obtained in the Ames 6×6 ft Supersonic Wind Tunnel, at Mach numbers from 0.4 to 0.925, at a unit Reynolds number of $10^7 m^{-1}$. The data obtained included surface pressure distributions from the midpoint of the bump aft, boundary-layer separation and reattachment locations using surface oil smear and oil dot techniques, and limited LDV profile data at the trailing edge of the bump.

Computations

The partial differential equations used to describe the mean flowfield are the time-dependent, Reynolds averaged, Navier-Stokes equations for axisymmetric flow of a compressible fluid. For the turbulence closure, the algebraic Cebeci-Smith[2] and the two-equation k-ϵ[3] turbulence models were used. A longitudinal curvature correction[4] was used with the k-ϵ model to determine whether its inclusion could improve the results. The numerical procedure used is the basic explicit second-order, predictor-corrector finite difference method of

Received Aug. 26, 1983; revision received Oct. 11,1983. This paper is declared a work of the U.S. Government and therefore is in the public domain.

*Research Scientist. Associate Fellow AIAA.
†Research Scientist. Member AIAA.

MacCormack, modified by an efficient implicit algorithm.[5] The computational domain extended in the flow direction from −140 to 90 cm and in the vertical direction from the model surface to 90 cm. A 129 × 45 mesh was developed that allowed a variable point spacing in each coordinate direction. In the streamwise direction, mesh spacing varied from 0.16 cm near the shock wave to 12 cm at the downstream boundary. Normal to the surface, an exponentially stretched spacing was used with the first mesh point from the model wall selected small enough so that the solutions are independent of spacing ($y^+_{min} < 1$).

The upstream boundary conditions were prescribed by uniform freestream conditions holding total pressure constant. At the downstream boundary all gradients in the flow direction were set to zero. No-slip bottom boundary conditions were applied at the model surface, along with a prescribed constant wall temperature. At the outer boundary, uniform freestream conditions were used, assuming the wind tunnel results were simulating free air results.

The computed results in Ref. 1 were made for solid-wall outer boundary conditions and a different numerical algorithm. At that time it was felt that axisymmetric solid-wall boundary conditions corresponding to a flow equivalent to that of the wind tunnel test best represented the wind tunnel data. However, the new data suggest that the wall interference was negligible and that a better outer boundary condition is free air. A new algorithm was used for the present solutions because it is easier to program and requires less computer CPU time for convergence. Solutions using the two algorithms, obtained for identical boundary conditions and turbulence models, were essentially identical.

Comparison of Navier-Stokes Solutions with Experiment

The experimental and computational results from Ref. 1 using solid wall boundary conditions are shown in Fig. 1. To demonstrate the effect of the outer boundary conditions, two additional computed results are shown using the same turbulence models and algorithm, but with free air boundary conditions. The new solutions show a forward movement of the shock wave and a change in the downstream pressure plateau level. These changes are significant because the new boundary conditions relieve the requirement of a locally high-speed flow over the bump. Although not shown here, results for the k-ϵ turbulence model differ little from the k-ω^2 results shown. The k-ϵ model was chosen for this study since the near wall analytic terms in the k-ω^2 model are not compatible with this algorithm.

The new experimental surface pressure coefficients are shown in Fig. 2 for freestream Mach numbers of 0.80, 0.85, 0.875, 0.90, and 0.925. The experimental separation and reattachment locations are shown in Fig. 3 for the same range of Mach numbers. Compared with these data are the computed results using the two-equation k-ϵ turbulence model with curvature (solid lines). Also shown in Fig. 2 for M= 0.875 and 0.90 are the computed pressure distributions for the k-ϵ model with no curvature corrections and the algebraic model.

The experimental pressure coefficient data show an increasing shock strength and subsequent pressure plateau with increasing Mach number. The shock wave location remains approximately the same. The separation length also increases with Mach number. Although the computed results show the same trends, it may be seen that the relatively good agreement between experiment and computations at the lower Mach numbers deteriorates at the higher Mach numbers. The computed shock wave location moves downstream from the experiment, and the pressure plateau is much less pronounced. Comparing separation lengths (Fig. 3), the computation shows no separation at M= 0.80, while the experiment shows a significant region of separation. The initial failure to predict the separated region for subcritical

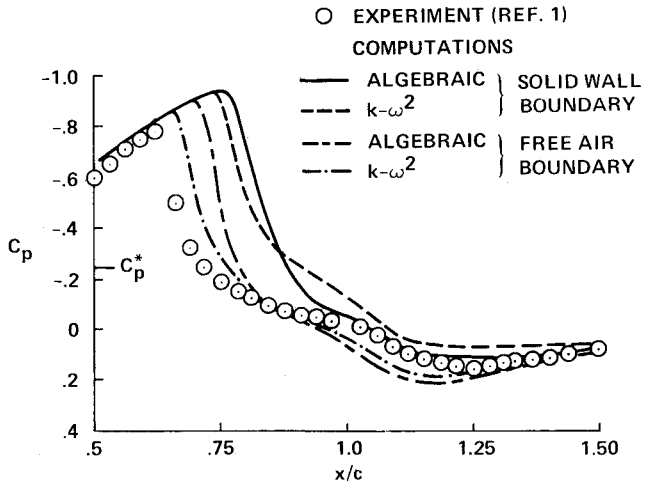

Fig. 1 Comparison of measured and computed surface pressure distributions using different farfield boundary conditions, M=0.875.

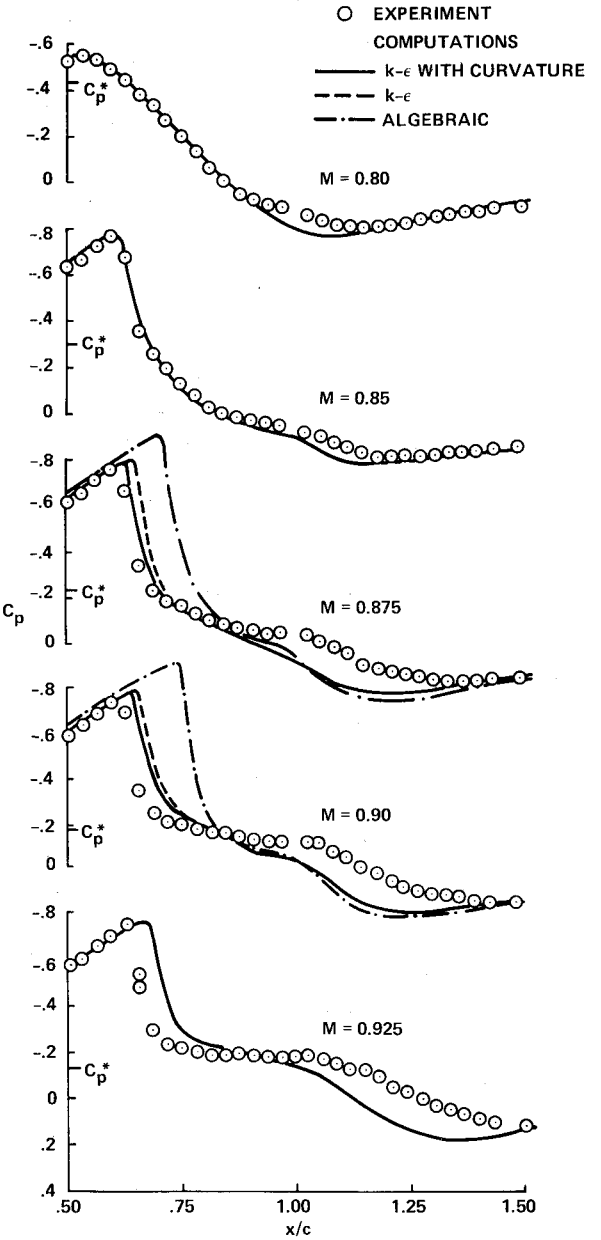

Fig. 2 Comparison of measured and computed surface pressure distributions.

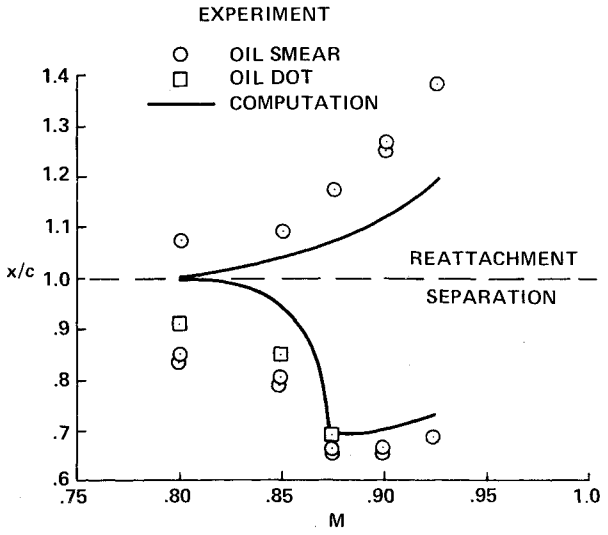

Fig. 3 Comparison of measured and computed separation zones.

conditions probably contributes to a general underprediction of the extent of separation for all subsequent higher Mach numbers. As the Mach number increases to 0.875 where shock-wave-induced separation is present, the computed separation locations are in good agreement with experiment. However, the experimental reattachment location is always significantly downstream of the computed values.

The turbulence model comparisons for the $M=0.875$ and 0.90 cases show that the curvature correction is not important, but the differences between the two-equation and algebraic models are. The algebraic model predicts a shock-wave location significantly downstream of the two-equation result but the shape of the pressure plateau is not too different. This is because the reattachment point for both models is nearly the same and the displacement thicknesses at $x/c=1$ only differ by 10%.

Conclusion

New data have been presented for a transonic shock-wave/boundary-layer interaction flow with separation for a range of freestream Mach numbers. Computed results using a two-equation eddy viscosity turbulence model showed reasonable agreement with the measured pressure distribution at the lower Mach numbers, but as the Mach number increased and the separated zone began to dominate the flowfield, the computations could not accurately predict the flowfield. For all Mach numbers, the length of separated zone was substantially underpredicted. Computed results using an algebraic turbulence model clearly showed these results to be inferior to the two-equation model computations.

References

[1] Johnson, D. A., Horstman, C. C., and Bachalo, W. D., "Comparison Between Experiment and Prediction for a Transonic Turbulent Separated Flow," *AIAA Journal,* Vol. 20, June 1982, pp. 737-744.

[2] Cebecci, T. and Smith, A. M. O., *Analysis of Turbulent Boundary Layers,* Academic Press, New York, 1974.

[3] Jones, W. P. and Launder, B. E., "The Prediction of Laminarization with a Two-Equation Model of Turbulence," *International Journal of Heat and Transfer,* Vol. 15, Feb. 1972, pp. 301-314.

[4] Kline, S. J., Cantwell, B. J.., and Lilley, G. M., eds., "The 1980-81 AFSOR/-HTTM-Stanford Conference on Complex Turbulent Flows: Comparison of Computation and Experiment," Vol. III, Stanford Univ., Stanford, Calif., 1982, pp. 1326-1336.

[5] MacCormack, R.W., "A Numerical Method for Solving the Equations of CompressibleViscous Flow," *AIAA Journal,* Vol. 20, Sept. 1982, pp. 1275-1281.

Nozzle Flow Using the Galerkin Finite Element Method

T. Doan* and R. D. Archer†
The University of New South Wales
New South Wales, Australia

Nomenclature

A	= cross-sectional area; or two-dimensional domain of solution
ℓ	= coordinate index; =0 Cartesian or =1 cylindrical coordinates
L_k, N_i	= shape functions
$\dot{m}$	= mass flow rate
n	= number of nodal points
p	= pressure
r,z	= radial and axial directions (Fig. 1)
R_*	= throat radius of curvature (Fig. 1)
S	= element boundary
t,n	= unit vectors tangential and normal to the surface
u,w,V	= radial, axial, and total velocity
γ	= specific heat ratio, =1.4
ρ	= fluid density
ω	= density correction factor[4]
∇	= divergence operator

Subscripts

i,j,k	= node number
in	= inlet, face AB (Fig. 1)
0	= stagnation condition

Introduction

THE Galerkin technique has opened up the application of the finite element method (FEM)[1] to fluid flow.[2] Consider the well-known problem[3] of steady, inviscid, compressible perfect gas flow in an arbitrarily shaped, axisymmetric nozzle. Many recent FEM solutions[4-6] to fluid flow problems have adopted the velocity potential (ϕ), or stream function (ψ), as dependent variables in the governing equations. Reference 7 simplifies the differential equations in each element by a local linearization process; Ref. 8 used groups of (primitive) variables, namely (ρu, ρw, ρuw), giving a system of nonlinear equations; and Ref. 9 employs a least-squares criterion on a system of two first-order equations, continuity and irrotationality, written in terms of (ρ,u,w).

Here, we report the results of the Galerkin FEM applied with linear shape functions to the equations of motion, Eqs. (1-4), in the primitive variables (ρ,u,w), combined with the irrotationality condition, Eq. (5).

Basic Equations and Assumptions

The nozzle (Fig. 1) is made up of a constant diameter inlet length and simple convergent-divergent cones, interconnected by sections whose wall shapes are circular arcs. In cylindrical (r,z) coordinates, the governing equations under steady-state conditions are as follows.

Received March 23, 1983; revision received Aug. 8, 1983.

*Graduate Student; currently, Engineer, Generation and Operations Department, Queensland Electricity Generation Board, Brisbane.

†Associate Professor, School of Mechanical and Industrial Engineering.